

Many-body interferometry of magnetic polaron dynamics

Yuto Ashida,¹ Richard Schmidt,^{2,3} Leticia Tarruell,⁴ and Eugene Demler³

¹*Department of Physics, University of Tokyo, 7-3-1 Hongo, Bunkyo-ku, Tokyo 113-0033, Japan*

²*ITAMP, Harvard-Smithsonian Center for Astrophysics, Cambridge, Massachusetts 02138, USA*

³*Department of Physics, Harvard University, Cambridge, Massachusetts 02138, USA*

⁴*ICFO-Institut de Ciències Fotòniques, The Barcelona Institute of Science and Technology, 08860 Castelldefels (Barcelona), Spain*

(Dated: October 30, 2018)

Strongly imbalanced mixtures of ultracold atoms open new possibilities for exploring impurity physics. Recent studies of impurities interacting with a single-component, degenerate gas provided new insights into the physics of Bose and Fermi polarons. Yet, measuring the polaron dressing cloud that is the ultimate building block of polarons remained a major challenge. Here we show that the Ramsey interferometry of bath atoms provide a way to directly probe the polaron-cloud formation dynamics. As an example, we demonstrate that an impurity atom immersed in a two-component Bose-Einstein condensate provides a unique platform to study magnetic polaron dynamics, where Ramsey interference of bath atoms enables a direct measurement of spin-wave excitations generated in the environment. This allows us to study the formation of magnetic polarons in real time and reveal an interplay of few- and many-body physics that is signified by single- and multi-frequency oscillatory spin dynamics corresponding to the formation of many-body bound states. We discuss concrete experimental implementations in ultracold atoms.

PACS numbers: 67.85.-d

Understanding the role of interactions between an impurity and its environment is a fundamental problem in quantum many-body physics. A central concept for the description of such systems is the formation of quasiparticle excitations called polarons [1]. Recent experimental realizations of imbalanced mixtures of ultracold atoms have opened up new possibilities for studying polaron physics in a highly controlled manner. Until now studies focused on impurities interacting with a single-component Bose-Einstein condensate (BEC) [2–28] or Fermi gas of atoms [29–42]. This allowed to study polaron dynamics beyond the Fröhlich paradigm and to take first steps to explore the physics of the Anderson orthogonality catastrophe [43–47].

Previously, studies in ultracold atoms focused on the spectroscopy of *impurities* to probe the polaron formation [5–14, 16, 19–26]. While such studies give new insights into properties of the dressed quasiparticles, they do not allow for observing “polaron cloud”, i.e., change in the environment arising from the interaction with the impurity atom, even though it constitutes the ultimate building block of polarons. For example, directly observing phonons created in the many-body environment remained beyond the reach of current experiments not only in ultracold atoms but also in solid-state physics. Moreover, in the previous studies where measurements act on the impurity itself, signal amplitudes are intrinsically limited by the impurity density. Here we show that the Ramsey interferometry acting on the *bath atoms* can overcome these obstacles. At the example of magnetic polarons, we demonstrate that this method gives enhanced signal-to-noise ratio in signatures of impurity physics and allows one to count the number of bath excitations forming the polaron dressing cloud. In contrast to an impurity coupled to phonons in which observing its cloud formation poses a major challenge, a magnetic polaron is a spin-polarized cloud created by modified spin configurations around the magnetic impu-

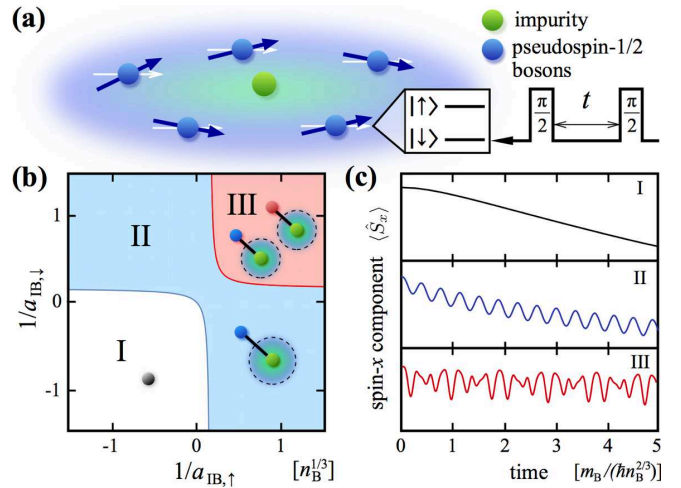


Figure 1. (a) Illustration of an impurity atom immersed in a two-component BEC. Arrows indicate the internal pseudospin states of BEC atoms. By applying a $\pi/2$ -pulse, the host bosons are initially prepared in an equal superposition of spin \uparrow - and \downarrow -state. The interaction between the impurity and host atoms induces spin dephasing, measurable by Ramsey interferometry. (b) Depending on the impurity-boson scattering lengths $a_{IB,\uparrow,\downarrow}$, the system is characterized by the existence of zero, one, and two many-body bound states (regions I, II, and III). The diagram is plotted for a boson-boson scattering length $a_{BBN_B}^{1/3} = 0.05$, and $m_1/m_B = 0.95$ as appropriate for a mixture of ^{41}K - ^{39}K atoms. (c) The BEC spin dephasing dynamics exhibits (I) monotone relaxation, (II) single- and (III) multi-frequency oscillations reflecting the existence of bound states. The dephasing signal is proportional to the number of impurities, which fixes the scale of the vertical axis.

riety [48] and it is this magnetic dressing that enables one to directly observe the polaron cloud. In a broader context, magnetic polarons determine thermodynamic and transport properties of many condensed matter systems including

doped magnetic semiconductors [49–51], metallic ferromagnets [52], high-temperature superconductors [53], ^3He - ^4He mixtures [54], and ferromagnetic perovskites [55, 56]. Technologically, magnetic polarons play a crucial role in magnetic solid state devices and are explored in spintronics [57, 58].

In this Letter, we show that the use of Ramsey interferometry performed on *bath atoms* allows a direct measurement of polaron-cloud formation in real time. Applying it to impurity atoms immersed in a two-species BEC, we propose a novel platform to explore impurities interacting with a magnetic environment and study the impact of the polaron formation on the many-body environment. The setup is illustrated in Fig. 1(a); the host BEC atoms provide an artificial ferromagnetic medium in which the impurity is dressed by spin-wave excitations leading to the formation of a magnetic polaron. Exploiting Ramsey interferometry on the *bath atoms*, one can directly measure the number of spin-wave excitations that reveals the real-time dynamics of the polaron-cloud formation. Our scheme can provide amplified signal per impurity because the impurity induces the creation of not only a single, but multiple spin excitations in the bath, which can be directly measured by Ramsey interferometry. This advantage has an application to a multitude of experimental systems in which interferometric schemes are readily available. Our approach thus suggests novel possibilities for efficiently probing impurity physics in a way different from the previous studies, where the impurity itself was probed either by radio-frequency [4, 17, 18, 29, 30, 35–37] or interferometric measurements [44–46, 59] and thus the signal amplitudes were intrinsically limited by the number of impurities.

While the dressing by spin-waves is the key signature of magnetic polarons, ultracold atoms also allow us to reveal impurity physics in the tunable strongly interacting regime that is not readily attainable in solid-state systems. As a striking feature of the strong-coupling physics, we find that the magnetic polaron forms many-body bound states with the BEC atoms. This leads to a unique ‘phase diagram’ of the magnetic-polaron system (Fig. 1(b)), which characterizes distinct oscillatory dynamics in the many-body environment (Fig. 1(c)).

Model.— We consider an impurity of mass m_I having no internal degrees of freedom and being immersed in a weakly interacting *two-component* spinor BEC of atoms of mass m_B (Fig. 1(a)). This is in contrast with the opposite situation of a two-level impurity interacting with a single-component BEC [11–14, 16–19]. The system is described by the Hamiltonian

$$\hat{H} = \hat{H}_B + \hat{V}_{IB} + \hat{H}_I, \quad (1)$$

where

$$\hat{H}_B = \sum_{\mathbf{k}\sigma} \epsilon_{\mathbf{k}} \hat{a}_{\mathbf{k}\sigma}^\dagger \hat{a}_{\mathbf{k}\sigma} + \frac{g_{BB}}{2V} \sum_{\mathbf{k}\mathbf{k}'\mathbf{q}\sigma\sigma'} \hat{a}_{\mathbf{k}+\mathbf{q}\sigma}^\dagger \hat{a}_{\mathbf{k}'-\mathbf{q}\sigma'}^\dagger \hat{a}_{\mathbf{k}'\sigma'} \hat{a}_{\mathbf{k}\sigma} \quad (2)$$

accounts for the background BEC of density n_B . The interac-

tion between the impurity and the host bosons is given by

$$\hat{V}_{IB} = \frac{1}{V} \sum_{\mathbf{k}\mathbf{q}\sigma} g_{IB,\sigma} \hat{a}_{\mathbf{k}+\mathbf{q}\sigma}^\dagger \hat{a}_{\mathbf{k}\sigma} e^{i\mathbf{q}\hat{\mathbf{R}}}, \quad (3)$$

and $\hat{H}_I = \hat{\mathbf{P}}^2/(2m_I)$ is the kinetic energy of the impurity. The operators $\hat{a}_{\mathbf{k}\sigma}$ ($\hat{a}_{\mathbf{k}\sigma}^\dagger$) annihilate (create) the host bosons with wavenumber \mathbf{k} and spin $\sigma = \uparrow, \downarrow$, and $\epsilon_{\mathbf{k}} = \hbar^2 \mathbf{k}^2/(2m_B)$ is their dispersion relation. The momentum (position) of the impurity is described by $\hat{\mathbf{P}}$ ($\hat{\mathbf{R}}$). We assume spin independent interactions between the host bosons characterized by the single parameter g_{BB} , as realized for many bosonic species [60]. In contrast, the interaction between the impurity and the bosons is spin dependent and given by $g_{IB,\sigma}$, which are related to the scattering lengths $a_{IB,\sigma}$ by the Lippmann-Schwinger equation [60].

First, the effective magnetic environment is created by an interferometric Ramsey protocol, where we initially prepare a superposition state of the pseudospin-1/2 BEC: $|\Psi_{BEC}\rangle \propto (\hat{a}_{0\uparrow}^\dagger + \hat{a}_{0\downarrow}^\dagger)^{N_B} |0\rangle$, with N_B being the number of the host bosons. A generalization to arbitrary spin rotations is straightforward. Due to the SU(2) symmetry of \hat{H}_B , the internal dynamics of the background bosons of homogeneous density causes no decoherence. In contrast, scattering with the impurity breaks this symmetry, which induces spin dephasing of the medium and triggers unique many-body dynamics.

Following a Bogoliubov approximation for the bosonic part of Eq. (1), we expand $\hat{a}_{\mathbf{k}\sigma}$ around $\langle \hat{a}_{0\sigma} \rangle = \sqrt{N_B/2}$, retain terms up to the second order, and diagonalize the bath Hamiltonian. Dealing with a two-component BEC, the resulting bosonic degrees of freedom correspond not only to phonon (‘charge’) excitations—as in the case of a single-component BEC—but also spin-wave (‘magnon’) excitations. It is the generation of the latter that leads to spin dephasing of the medium on the one hand, and dressing of the impurity by magnons on the other. Transforming to the frame comoving with the polaron [61], we obtain the effective Hamiltonian [60]:

$$\begin{aligned} \hat{\mathcal{H}} = & g_{IB}^+ n_B + \frac{(\hat{\mathbf{P}} - \hat{\mathbf{P}}_B)^2}{2m_I} + \sum_{\mathbf{k}} \left(\epsilon_{\mathbf{k}}^c \hat{\gamma}_{\mathbf{k}}^{\dagger c} \hat{\gamma}_{\mathbf{k}}^c + \epsilon_{\mathbf{k}}^s \hat{\gamma}_{\mathbf{k}}^{\dagger s} \hat{\gamma}_{\mathbf{k}}^s \right) \\ & + \sqrt{\frac{n_B}{V}} \sum_{\mathbf{k}} \left[g_{IB}^+ W_{\mathbf{k}} \left(\hat{\gamma}_{\mathbf{k}}^c + \hat{\gamma}_{-\mathbf{k}}^{\dagger c} \right) + g_{IB}^- \left(\hat{\gamma}_{\mathbf{k}}^s + \hat{\gamma}_{-\mathbf{k}}^{\dagger s} \right) \right] \\ & + \frac{g_{IB}^+}{2V} \sum_{\mathbf{k}, \mathbf{k}'} \left(V_{\mathbf{k}\mathbf{k}'}^{\dagger c} \hat{\gamma}_{\mathbf{k}}^{\dagger c} \hat{\gamma}_{\mathbf{k}'}^c + \hat{\gamma}_{\mathbf{k}}^{\dagger s} \hat{\gamma}_{\mathbf{k}'}^s + V_{\mathbf{k}\mathbf{k}'}^{\dagger c} \hat{\gamma}_{\mathbf{k}}^{\dagger c} \hat{\gamma}_{\mathbf{k}'}^c + \text{H.c.} \right) \\ & + \frac{g_{IB}^-}{V} \sum_{\mathbf{k}, \mathbf{k}'} \left(u_{\mathbf{k}} \hat{\gamma}_{\mathbf{k}'}^{\dagger s} \hat{\gamma}_{\mathbf{k}}^c - v_{\mathbf{k}} \hat{\gamma}_{\mathbf{k}'}^{\dagger s} \hat{\gamma}_{\mathbf{k}}^{\dagger c} + \text{H.c.} \right). \end{aligned} \quad (4)$$

Here, $\hat{\mathbf{P}}$ in this frame represents the total momentum of the system (we consider the case $\hat{\mathbf{P}} = 0$ hereafter), $\hat{\mathbf{P}}_B = \sum_{\mathbf{k}} \hbar \mathbf{k} (\hat{\gamma}_{\mathbf{k}}^{\dagger c} \hat{\gamma}_{\mathbf{k}}^c + \hat{\gamma}_{\mathbf{k}}^{\dagger s} \hat{\gamma}_{\mathbf{k}}^s)$, $\epsilon_{\mathbf{k}}^c = \sqrt{\epsilon_{\mathbf{k}} (\epsilon_{\mathbf{k}} + 2g_{BB}n_B)}$ and $\epsilon_{\mathbf{k}}^s = \hbar^2 \mathbf{k}^2/(2m_B)$ are the total boson momentum and the dispersion relations of the charge and spin wave excitations, respectively. The excitations are annihilated (created) by the

operators, $\hat{\gamma}_\mathbf{k}^{c,s}$ ($\hat{\gamma}_\mathbf{k}^{\dagger c,s}$) that obey the commutation relations $[\hat{\gamma}_\mathbf{k}^\xi, \hat{\gamma}_\mathbf{k}^\eta] = [\hat{\gamma}_\mathbf{k}^{\dagger\xi}, \hat{\gamma}_\mathbf{k}^{\dagger\eta}] = 0$, and $[\hat{\gamma}_\mathbf{k}^\xi, \hat{\gamma}_\mathbf{k}'^{\dagger\eta}] = \delta_{\xi,\eta} \delta_{\mathbf{k},\mathbf{k}'}$ with $\xi, \eta = s, c$. We introduce the vertices $W_\mathbf{k} = \sqrt{\epsilon_\mathbf{k}/\epsilon_\mathbf{k}^c}$, $V_{\mathbf{k}\mathbf{k}'}^{(1)} \pm V_{\mathbf{k}\mathbf{k}'}^{(2)} = (W_\mathbf{k} W_{\mathbf{k}'})^{\pm 1}$, as well as $u_\mathbf{k}$ and $v_\mathbf{k}$ as the coefficients of the Bogoliubov transformation. We also introduce the average and difference of the interaction parameters as $g_{IB}^\pm = (g_{IB,\uparrow} \pm g_{IB,\downarrow})/2$. When $g_{IB}^- \neq 0$, the imbalance in the impurity-boson interactions switches on spin-charge interactions and generates spin waves. While the first two lines in Eq. (4) describe the generalization of Fröhlich polaron-type physics [62] to magnon dynamics, the last two lines account for the strong coupling physics that leads to the formation of magnetic polaron bound states.

The magnetic many-body dynamics of the system can be probed through Ramsey interference. Starting with a bath in the \uparrow state, a first $\pi/2$ pulse is used to prepare a superposition of \uparrow and \downarrow . After the system is evolved for a time t , an additional $\pi/2$ pulse is applied and the difference between the populations of atoms in the \uparrow and \downarrow states is measured. In this way, the spin- x component $\hat{S}_x = (\hbar/2) \sum_{\mathbf{k}\mu\nu} \hat{a}_{\mathbf{k}\mu}^\dagger \sigma_{\mu\nu}^x \hat{a}_{\mathbf{k}\nu}$ is determined, with σ^x being the Pauli matrix. This is directly related to the spin-excitation number $N^s(t) = \sum_\mathbf{k} \langle \hat{\gamma}_\mathbf{k}^\dagger s \hat{\gamma}_\mathbf{k}^s \rangle$ as

$$\langle \hat{S}_x \rangle = \frac{1}{2} - \frac{N^s(t)}{N_B}. \quad (5)$$

Time-dependent variational approach.— To study the dynamics of the system, we invoke the time-dependent variational approach [63]. In particular, we employ a projection onto the submanifold of the Hilbert space spanned by the product of coherent states

$$|\Psi(t)\rangle = e^{\sum_\mathbf{k} (\alpha_\mathbf{k}^c(t) \hat{\gamma}_\mathbf{k}^c + \alpha_\mathbf{k}^s(t) \hat{\gamma}_\mathbf{k}^s - h.c.)} |0\rangle, \quad (6)$$

where $\alpha_\mathbf{k}^{c,s}(t)$ are the time-dependent amplitudes of the charge and spin excitations and $|0\rangle$ is their vacuum. The state (6) gives the exact solution for an impurity of infinite mass immersed into an ideal BEC. Thus, our ansatz is based on an exact limit that holds regardless of the interaction strength between the impurity and host bosons.

The equations of motion for $\alpha_\mathbf{k}^{c,s}$ are given by the variational condition $\delta[\langle \Psi | i\hbar\partial_t - \hat{\mathcal{H}} | \Psi \rangle] = 0$, which results in the coupled integral equations:

$$i\hbar\partial_t \begin{pmatrix} \alpha^c \\ \alpha^s \end{pmatrix} = \mathcal{M} \begin{pmatrix} \alpha^c \\ \alpha^s \end{pmatrix} + \mathcal{F}, \quad (7)$$

where the matrix \mathcal{M} and vector \mathcal{F} are independent of $\alpha_\mathbf{k}^{c,s}$ [60]. The stationary solution $|\Psi_{\text{mpol}}\rangle$ of Eq. (S4) contains non-zero spin and charge excitations and represents the magnetic dressed polaron with energy $E_{\text{mpol}} = \langle \Psi_{\text{mpol}} | \hat{\mathcal{H}} | \Psi_{\text{mpol}} \rangle$.

Quantum spin dynamics.— The formation of magnetic polarons leads to distinct quantum spin dynamics in the bosonic medium. Figure 2 shows the number of spin and charge excitations $N^{s,c}(t)$ for different scattering lengths $a_{IB,\sigma}$ in the

regions I, II, and III, where the system supports zero, one, and two bound states (Fig. 1(b)). In the absence of bound states, $N^s(t)$ grows as $\propto \sqrt{t}$ at long times, while $N^c(t)$ eventually saturates (panel I in Fig. 2). As a consequence, the number of spin excitations per impurity will easily exceed one, which can be directly probed by measuring the population of atoms remaining in the \uparrow state after the Ramsey protocol (see Eq. (5)). It is this amplification that can effectively improve the signal-to-noise ratio of the measurement. Thus, interferometric probes acting *on the bath* provide a novel way to amplify experimental signatures of impurities, in sharp contrast to the conventional spectroscopic [4, 17, 18, 29, 30, 35–37] or interferometric methods [44–46, 59] whose signal amplitudes are intrinsically limited by the impurity density.

The unbounded generation of spin waves originates from the quadratic nature of the magnon dispersion relation [60]. Importantly, collective excitations having quadratic low-energy dispersion ubiquitously appear in many other setups such as fermionic gases [64, 65], multi-component Bose-Einstein condensates [66, 67], and Rydberg or dipolar gases [68–70]. This fact shows the broad applicability of our approach since interferometric tools of atomic spectroscopy are readily available in these vastly different systems.

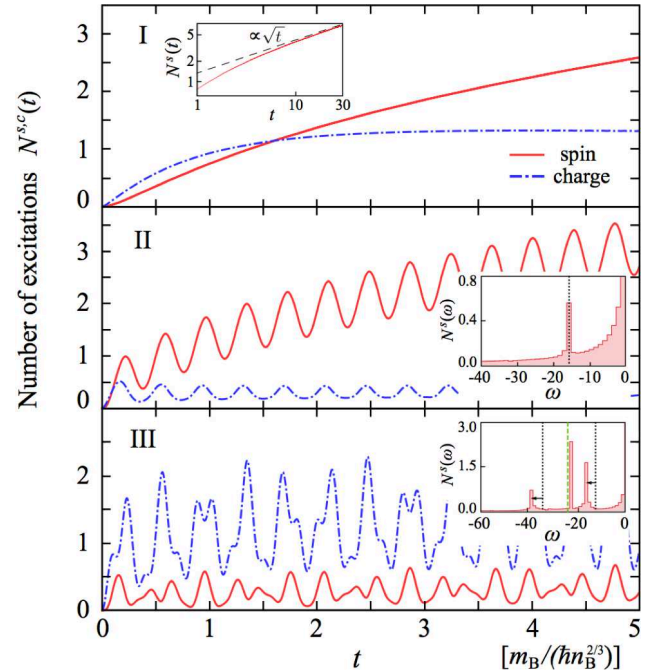


Figure 2. Quantum dynamics of bath spin (red solid line) and charge (blue dashed line) excitations for a single impurity immersed in a two-component BEC. The impurity-boson scattering lengths are $n_B^{1/3}(a_{IB,\uparrow}, a_{IB,\downarrow}) = (-1, -10)$ in I, $(3.5, -5)$ in II, and $(3.5, 5)$ in III. The inset in I shows the long-time behavior of spin excitations approaching an asymptotic \sqrt{t} scaling. The insets in II and III show the Fourier spectra of $N^s(t)$. The energies of the underlying bound states and their difference, calculated from Eq. (9), are shown as black dotted lines and green dashed lines, respectively.

Magnetic dressed bound states.— The presence of bound states triggers single- and multi-frequency oscillations in the number of the spin and charge excitations (panels II and III in Fig. 2). This reflects the formation and coupling of many-body bound states. To gain further insights, we consider the variational wavefunction

$$|\Psi_b(t)\rangle = \sum_{\mathbf{k}} \left(\psi_{\mathbf{k}}^c(t) \hat{\gamma}_{\mathbf{k}}^{\dagger c} + \psi_{\mathbf{k}}^s(t) \hat{\gamma}_{\mathbf{k}}^{\dagger s} \right) |\Psi_{\text{mpol}}\rangle, \quad (8)$$

which accounts for bound states consisting of single spin-charge excitations bound to the magnetic polaron, i.e., the collective object of the impurity dressed by surrounding many-body excitations (see Fig. 1(b)). We determine the eigenmodes $\psi_{\mathbf{k}}^{c,s} \propto e^{-i\omega t}$ of the equation of motion for the state (8) which yields the eigenvalue equation [60]

$$(a_{\text{IB}}^-)^2 = [a_{\text{IB}}^+ - l_s(\omega, a_{\text{IB}}^+)] [a_{\text{IB}}^+ - l_c(\omega, a_{\text{IB}}^+)]. \quad (9)$$

Here $a_{\text{IB}}^{\pm} = (a_{\text{IB},\uparrow} \pm a_{\text{IB},\downarrow})/2$ and $1/l_{s,c} = (2\pi/m_{\text{red}})(2m_{\text{red}} \sum_{\mathbf{k}} (1/\mathbf{k}^2) + \hbar^2 \Pi_{s,c})$, which, together with

$$\Pi_s = \sum_{\mathbf{k}} \frac{1}{\hbar\omega - E_{\text{mpol}} - \Omega_{\mathbf{k}}^s}, \quad \Pi_c = \sum_{\mathbf{k}} \frac{(W_{\mathbf{k}}^2 + W_{\mathbf{k}}^{-2})/2}{\hbar\omega - E_{\text{mpol}} - \Omega_{\mathbf{k}}^c}, \quad (10)$$

are fully regularized expressions ($\Omega_{\mathbf{k}}^{s,c} = \hbar^2 \mathbf{k}^2 / (2m_I) + \epsilon_{\mathbf{k}}^{s,c}$). Depending on the scattering lengths $a_{\text{IB},\sigma}$, Eq. (9) has zero, one, or two solutions determining the phase boundaries in Fig. 1(b). The latter are modified with respect to the corresponding two-body problem reflecting the many-body character of the bound states. In the two-particle problem, a dimer bound state of energy $\epsilon_{\text{dim}} = \hbar^2 / (2m_{\text{red}} a_{\text{IB},\sigma}^2)$ ($m_{\text{red}} = m_I m_B / (m_I + m_B)$) exists for positive scattering length $a_{\text{IB},\sigma}$, and thus there are two distinct regions for each individual bound state: the impurity bound to a host \uparrow -boson, or the impurity bound to a host \downarrow -boson. Remarkably, the many-body phase diagram in Fig. 1(b) does not show the corresponding four distinct regimes. Instead, the exchange of magnetic excitations hybridizes the bound states with the medium, resulting in a unified region II.

In this region II, we find that the oscillation frequency governing the bath-spin dynamics agrees with the bound-state energy calculated from Eq. (9) (inset of panel II in Fig. 2). In contrast, when two bound states are present (region III), the bath-induced coupling between those manifests itself as a shift in the oscillation frequencies from the bound-state energies as well as a large peak at the difference of these two energy scales (inset of panel III in Fig. 2). This effect can be understood in terms of a polaronic nonlinearity introduced by the magnetic medium [71], which induces strongly coupled oscillators dynamics, analogous to polariton-polariton interactions [72] and competing orders in strongly correlated electrons [73]. As we depart from the strongly interacting regime, the coupling of the two bound states weakens and the oscillation frequencies eventually converge to the bound-state energies given by

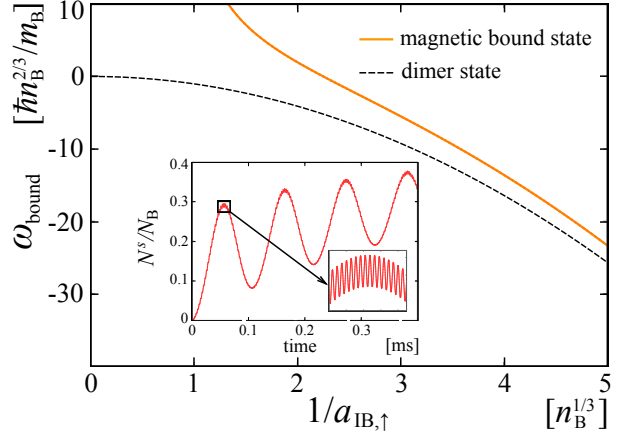


Figure 3. The magnetic bound-state energy ω_{bound} (solid line) calculated from Eq. (9), and the bare dimer energy $\epsilon_{\text{dim}} = \hbar^2 / (2m_{\text{red}} a_{\text{IB},\uparrow}^2)$ (dashed line) are plotted against the inverse impurity-bath scattering length $1/a_{\text{IB},\uparrow}$. The inset shows the dynamics of spin excitations at $1/(a_{\text{IB},\uparrow} n_B^{1/3}) = 2$ where we assume a homogeneous density $n_B = 10^{14} \text{ cm}^{-3}$, and a finite impurity density $n_I/n_B = 0.1$. We choose $a_{\text{BB}} n_B^{1/3} = 0.05$, and set $1/(a_{\text{IB},\downarrow} n_B^{1/3}) = 15$ and $m_I/m_B = 0.95$ as appropriate for a ^{41}K - ^{39}K mixture.

Eq. (9) [60]. These findings suggest that energies of underlying *few-body* bound states can be measured by studying the *many-body* response of the medium yielding enhanced signal-to-noise ratio.

Experimental implementation.— A large number of Bose-Bose and Bose-Fermi mixtures allow for the observation of magnetic polaron physics. As one possible example, we consider here a Bose-Bose mixture of ^{41}K - ^{39}K atoms. We identify two miscible states $|\uparrow\rangle = |F = 1, m_F = 1\rangle$ and $|\downarrow\rangle = |F = 1, m_F = 0\rangle$ of ^{41}K as the host bosons and $|i\rangle = |F = 1, m_F = 1\rangle$ of ^{39}K as the impurity. In this case, the $|\uparrow\rangle - |i\rangle$ interaction can be tuned using a Feshbach resonance at 500 G [74]. The imbalance in the scattering lengths of the two-component host bosons is less than 0.4% [75]. While such a small breaking of the SU(2) symmetry can in general induce decoherence of the atomic spins, we demonstrate in [60] that the effect is negligible compared with the spin dynamics induced by the impurities.

In Fig. 3, we plot the energy ω_{bound} of the magnetic-dressed bound state as calculated from Eq. (9). The result is shown in the vicinity of a Feshbach resonance where $a_{\text{IB},\uparrow}$ takes a large positive value, while $a_{\text{IB},\downarrow}$ is determined by a small, positive background value. This significant imbalance in scattering lengths creates a large number of spin excitations in the bath, which can exceed the number of impurities. Furthermore, the underlying shallow bound state triggers oscillatory spin dynamics. Both features can be seen in the inset of Fig. 3. For typical experimental parameters, we predict the time evolution of $N^s(t)$, which can be measured as the fraction of bath atoms residing in the \uparrow -state at the end of the Ramsey sequence (see Eq. (5)), resulting in the

oscillation frequency ~ 10 kHz. These effects should thus be readily accessible in current experiments [76]. Note that, although the contribution to the dynamics from the second, deeply bound state associated with a small positive $a_{IB,\downarrow}$ is significantly suppressed, it is manifest as a tiny, fast beating on top of the ‘slow’ magnetic bound state oscillations. While we have considered here an isotopic potassium mixture, there are other candidates for bath atoms such as ^{87}Rb and ^{23}Na , where the imbalance in the scattering lengths can be small enough to observe the predicted phenomena [60, 77, 78].

Conclusions and Outlook.— We showed that the real-time dynamics of polaron-cloud formation can be directly probed by employing the many-body Ramsey interferometry of bath atoms around the impurity. Analyzing an impurity immersed in a two-component Bose gas as an example, we demonstrated that the generation of spin excitations is the key signature of magnetic-polaron formation and found that the medium spins exhibit characteristic oscillatory behavior governed by the underlying bound states. The proposed interferometric scheme can enhance the signature of impurities, which has a general applicability to a variety of systems in which the low-energy excitation is quadratic and interferometric tools are readily available. This leads to a novel route for observing few-body physics beyond conventional spectroscopy [4, 17, 18] and loss measurements [79] whose signal amplitudes are intrinsically limited by the number of impurities.

A generalization to large spin spinor BECs [80] and a use of *in-situ* imaging techniques [81–85] can provide new insights in polaron and spin physics. It remains an open question how the nature of the polarons changes as the impurity density increases to such a degree that magnon-mediated interaction [86] becomes important, potentially leading to a superconducting instability of a fermionic polaron gas.

Acknowledgements.— We acknowledge F. Grusdt, Y. Shchadilova, M. Tomza, M. Ueda, G. Zar  nd for fruitful discussions. The authors acknowledge support from the NSF Grant No. DMR-1308435, Harvard-MIT CUA, AFOSR New Quantum Phases of Matter MURI, the ARO-MURI on Atomtronics, ARO MURI Quism program. Y.A. acknowledges support from the Japan Society for the Promotion of Science through Program for Leading Graduate Schools (ALPS) and Grant No. JP16J03613, and Harvard University for hospitality, where this work was completed. R.S. is supported by the NSF through a grant for the Institute for Theoretical Atomic, Molecular, and Optical Physics at Harvard University and the Smithsonian Astrophysical Observatory. L.T. acknowledges support from Fundaci   Cellex, Spanish MINECO (FIS2014-59546-P and SEV-2015-0522) and EU (PCIG13-GA-2013 No. 631633 and H2020-FETPROACT-2014 No. 641122).

[1] G. Mahan, *Many-Particle Physics* (Kluwer Academic/Plenum Publishers, New York, 2000).

[2] L. Mathey, D. W. Wang, W. Hofstetter, M. D. Lukin, and E. Demler, *Phys. Rev. Lett.* **93**, 120404 (2004).

[3] S. Palzer, C. Zipkes, C. Sias, and M. K  hl, *Phys. Rev. Lett.* **103**, 150601 (2009).

[4] C.-H. Wu, J. W. Park, P. Ahmadi, S. Will, and M. W. Zwierlein, *Phys. Rev. Lett.* **109**, 085301 (2012).

[5] F. M. Cucchietti and E. Timmermans, *Phys. Rev. Lett.* **96**, 210401 (2006).

[6] A. Klein, M. Bruderer, S. R. Clark, and D. Jaksch, *New J. Phys.* **9**, 411 (2007).

[7] J. Tempere, W. Casteels, M. K. Oberthaler, S. Knoop, E. Timmermans, and J. T. Devreese, *Phys. Rev. B* **80**, 184504 (2009).

[8] W. Casteels, J. Tempere, and J. T. Devreese, *Phys. Rev. A* **84**, 063612 (2011).

[9] N. Spethmann, F. Kindermann, S. John, C. Weber, D. Meschede, and A. Widera, *Phys. Rev. Lett.* **109**, 235301 (2012).

[10] W. Casteels, J. Tempere, and J. T. Devreese, *Phys. Rev. A* **88**, 013613 (2013).

[11] S. P. Rath and R. Schmidt, *Phys. Rev. A* **88**, 053632 (2013).

[12] W. Li and S. Das Sarma, *Phys. Rev. A* **90**, 013618 (2014).

[13] R. S. Christensen, J. Levinsen, and G. M. Bruun, *Phys. Rev. Lett.* **115**, 160401 (2015).

[14] L. A. P. Ardila and S. Giorgini, *Phys. Rev. A* **92**, 033612 (2015).

[15] L. A. P. n. Ardila and S. Giorgini, *Phys. Rev. A* **94**, 063640 (2016).

[16] J. Levinsen, M. M. Parish, and G. M. Bruun, *Phys. Rev. Lett.* **115**, 125302 (2015).

[17] M.-G. Hu, M. J. Van de Graaff, D. Kedar, J. P. Corson, E. A. Cornell, and D. S. Jin, *Phys. Rev. Lett.* **117**, 055301 (2016).

[18] N. B. J  rgensen, L. Wacker, K. T. Skalmstang, M. M. Parish, J. Levinsen, R. S. Christensen, G. M. Bruun, and J. J. Arlt, *Phys. Rev. Lett.* **117**, 055302 (2016).

[19] Y. E. Shchadilova, R. Schmidt, F. Grusdt, and E. Demler, *Phys. Rev. Lett.* **117**, 113002 (2016).

[20] F. Grusdt, Y. E. Shchadilova, a. N. Rubtsov, and E. Demler, *Sci. Rep.* **5**, 12124 (2015).

[21] J. Vlietinck, W. Casteels, K. Van Houcke, J. Tempere, J. Ryckebusch, and J. T. Devreese, *New J. Phys.* **17**, 33023 (2015).

[22] R. Schmidt and M. Lemeshko, *Phys. Rev. Lett.* **114**, 203001 (2015).

[23] A. G. Volosniev, H.-W. Hammer, and N. T. Zinner, *Phys. Rev. A* **92**, 023623 (2015).

[24] Y. E. Shchadilova, F. Grusdt, A. N. Rubtsov, and E. Demler, *Phys. Rev. A* **93**, 043606 (2016).

[25] R. Schmidt and M. Lemeshko, *Phys. Rev. X* **6**, 011012 (2016).

[26] R. Schmidt, H. R. Sadeghpour, and E. Demler, *Phys. Rev. Lett.* **116**, 105302 (2016).

[27] F. F. Bellotti, T. Frederico, M. T. Yamashita, D. V. Fedorov, A. S. Jensen, and N. T. Zinner, *New J. Phys.* **18**, 043023 (2016).

[28] B. Midya, M. Tomza, R. Schmidt, and M. Lemeshko, *Phys. Rev. A* **94**, 041601 (2016).

[29] A. Schirotzek, C.-H. Wu, A. Sommer, and M. W. Zwierlein, *Phys. Rev. Lett.* **102**, 230402 (2009).

[30] S. Nascimb  ne, N. Navon, K. J. Jiang, L. Tarruell, M. Tichmann, J. McKeever, F. Chevy, and C. Salomon, *Phys. Rev. Lett.* **103**, 170402 (2009).

[31] X. Cui and H. Zhai, *Phys. Rev. A* **81**, 041602 (2010).

[32] R. Schmidt and T. Enss, *Phys. Rev. A* **83**, 063620 (2011).

[33] P. Massignan and G. M. Bruun, *Eur. Phys. J. D* **65**, 83 (2011).

[34] R. Schmidt, T. Enss, V. Pietil  , and E. Demler, *Phys. Rev. A* **85**, 021602 (2012).

[35] M. Koschorreck, D. Pertot, E. Vogt, B. Frohlich, M. Feld, and M. Köhl, *Nature* **485**, 619 (2012).

[36] C. Kohstall, M. Zaccanti, M. Jag, A. Trenkwalder, P. Massignan, G. M. Bruun, F. Schreck, and R. Grimm, *Nature* **485**, 615 (2012).

[37] Y. Zhang, W. Ong, I. Arakelyan, and J. E. Thomas, *Phys. Rev. Lett.* **108**, 235302 (2012).

[38] C. J. M. Mathy, M. B. Zvonarev, and E. Demler, *Nature Phys.* **8**, 881 (2012).

[39] P. Massignan, M. Zaccanti, and G. M. Bruun, *Rep. Prog. Phys.* **77**, 034401 (2014).

[40] W. Yi and X. Cui, *Phys. Rev. A* **92**, 013620 (2015).

[41] W. Ong, C. Cheng, I. Arakelyan, and J. E. Thomas, *Phys. Rev. Lett.* **114**, 110403 (2015).

[42] F. Meinert, M. Knap, E. Kirilov, K. Jag-Lauber, M. B. Zvonarev, E. Demler, and H.-C. Nägerl, *arXiv:1608.08200* (2016).

[43] M. Knap, A. Kantian, T. Giamarchi, I. Bloch, M. D. Lukin, and E. Demler, *Phys. Rev. Lett.* **111**, 147205 (2013).

[44] M. Cetina, M. Jag, R. S. Lous, J. T. M. Walraven, R. Grimm, R. S. Christensen, and G. M. Bruun, *Phys. Rev. Lett.* **115**, 135302 (2015).

[45] M. Cetina, M. Jag, R. S. Lous, I. Fritzsche, J. T. M. Walraven, R. Grimm, J. Levinsen, M. M. Parish, R. Schmidt, M. Knap, and E. Demler, *Science* **354**, 96 (2016).

[46] R. Schmidt, M. Knap, D. A. Ivanov, J.-S. You, M. Cetina, and E. Demler, *arXiv:1702.08587* (2017).

[47] F. Scazza, G. Valtolina, P. Massignan, A. Recati, A. Amico, A. Burchianti, C. Fort, M. Inguscio, M. Zaccanti, and G. Roati, *Phys. Rev. Lett.* **118**, 083602 (2017).

[48] P. G. de Gennes, *Phys. Rev.* **118**, 141 (1960).

[49] T. Kasuya and A. Yanase, *Rev. Mod. Phys.* **40**, 684 (1968).

[50] J. K. Furdyna and J. Kossut, eds., *Semiconductors and Semimetals* (Academic, London, 1988).

[51] T. Jungwirth, J. Sinova, J. Mašek, J. Kučera, and A. H. MacDonald, *Rev. Mod. Phys.* **78**, 809 (2006).

[52] P. Majumdar and P. B. Littlewood, *Nature* **395**, 479 (1998).

[53] E. K. H. Salje, A. S. Alexandrov, and W. Y. Liang, eds., *Polarons and Bipolarons in High Temperature Superconductors and Related Materials* (Cambridge University Press, Cambridge, 2005).

[54] J. Bardeen, G. Baym, and D. Pines, *Phys. Rev.* **156**, 207 (1967).

[55] R. von Helmolt, J. Wecker, B. Holzapfel, L. Schultz, and K. Samwer, *Phys. Rev. Lett.* **71**, 2331 (1993).

[56] J. M. De Teresa, M. R. Ibarra, P. A. Algarabel, C. Ritter, C. Marquina, J. Blasco, J. Garcia, A. del Moral, and Z. Arnold, *Nature* **386**, 256 (1997).

[57] S. Watanabe, K. Ando, K. Kang, S. Mooser, Y. Vaynzof, H. Kurebayashi, E. Saitoh, and H. Siringhaus, *Nature Phys.* **10**, 308 (2014).

[58] A. V. Chumak, V. I. Vasyuchka, A. A. Serga, and B. Hillebrands, *Nature Phys.* **11**, 453 (2015).

[59] M. M. Parish and J. Levinsen, *Phys. Rev. B* **94**, 184303 (2016).

[60] See Supplemental Material for details about experimental conditions and the derivations.

[61] T. Lee, F. Low, and D. Pines, *Phys. Rev.* **341**, 297 (1953).

[62] H. Fröhlich, *Adv. Phys.* **3**, 325 (1954).

[63] R. Jackiw and A. Kerman, *Phys. Lett. A* **71**, 1 (1979).

[64] A. Mazurenko, C. S. Chiu, G. Ji, M. F. Parsons, M. Kanász-Nagy, R. Schmidt, F. Grusdt, E. Demler, D. Greif, and M. Greiner, *Nature* **545**, 462 (2017).

[65] G. Valtolina, F. Scazza, A. Amico, A. Burchianti, A. Recati, T. Enss, M. Inguscio, M. Zaccanti, and G. Roati, *Nature Phys.* **13**, 704 (2017).

[66] A. V. Gorshkov, M. Hermele, V. Gurarie, C. Xu, P. S. Julienne, J. Ye, P. Zoller, E. Demler, M. D. Lukin, and A. M. Rey, *Nature Phys.* **6**, 289 (2010).

[67] G. E. Marti, A. MacRae, R. Olf, S. Lourette, F. Fang, and D. M. Stamper-Kurn, *Phys. Rev. Lett.* **113**, 155302 (2014).

[68] J. Zeiher, R. Van Bijnen, P. Schauß, S. Hild, J.-y. Choi, T. Pohl, I. Bloch, and C. Gross, *Nature Phys.* **12**, 1095 (2016).

[69] F. Böttcher, A. Gaj, K. M. Westphal, M. Schlagmüller, K. S. Kleinbach, R. Löw, T. C. Liebisch, T. Pfau, and S. Hofferberth, *Phys. Rev. A* **93**, 032512 (2016).

[70] D. Petrosyan, *New J. Phys.* **19**, 033001 (2017).

[71] S. Aubry, *Physica D* **103**, 201 (1997).

[72] N. A. Gippius, I. A. Shelykh, D. D. Solnyshkov, S. S. Gavrilov, Y. G. Rubo, A. V. Kavokin, S. G. Tikhodeev, and G. Malpuech, *Phys. Rev. Lett.* **98**, 236401 (2007).

[73] S. Pathak, V. B. Shenoy, M. Randeria, and N. Trivedi, *Phys. Rev. Lett.* **102**, 027002 (2009).

[74] Note that our calculation does not take into account finite range effects, which might become important for this particular resonance.

[75] M. Tomza, Private communications.

[76] An experimental aspect to be considered is the density dependence of ω_{bound} , which is expected to lead to a trap-density-averaging of the oscillations. This effect could be suppressed by localizing the impurities around the center of the system [45] or by performing local measurements [47].

[77] E. G. M. van Kempen, S. J. J. M. F. Kokkelmans, D. J. Heinzen, and B. J. Verhaar, *Phys. Rev. Lett.* **88**, 093201 (2002).

[78] C. Samuelis, E. Tiesinga, T. Laue, M. Elbs, H. Knöckel, and E. Tiemann, *Phys. Rev. A* **63**, 012710 (2000).

[79] P. Naidon and S. Endo, *Rep. Prog. Phys.* **80**, 056001 (2017).

[80] D. M. Stamper-Kurn and M. Ueda, *Rev. Mod. Phys.* **85**, 1191 (2013).

[81] W. S. Bakr, J. I. Gillen, A. Peng, S. Fölling, and M. Greiner, *Nature* **462**, 74 (2009).

[82] J. F. Sherson, C. Weitenberg, M. Endres, M. Cheneau, I. Bloch, and S. Kuhr, *Nature* **467**, 68 (2010).

[83] Y. Ashida and M. Ueda, *Phys. Rev. Lett.* **115**, 095301 (2015).

[84] Y. Ashida and M. Ueda, *Opt. Lett.* **41**, 72 (2016).

[85] A. Alberti, C. Robens, W. Alt, S. Brakhane, M. Karski, R. Reimann, A. Widera, and D. Meschede, *New J. Phys.* **18**, 053010 (2016).

[86] P. Naidon, *arXiv:1607.04507* (2016).

Supplementary Materials

Derivation of the effective Hamiltonian

We first derive the effective Hamiltonian given by Eq. (4) in the main text. To take into account the initial macroscopic population of the host bosons in the $\mathbf{k} = 0$ mode, we expand $\hat{a}_{0\sigma}$ around $\langle \hat{a}_{0\sigma} \rangle = \sqrt{N_B/2}$. Here the factor of 1/2 accounts for the fact that the bosons are prepared in a superposition of \uparrow - and \downarrow -states. We then diagonalize the bath Hamiltonian (Eq. (2) in the main text) using the Bogoliubov transformation:

$$\hat{a}_{\mathbf{k},\uparrow} = \frac{1}{\sqrt{2}} \left(\hat{\gamma}_{\mathbf{k}}^s + u_{\mathbf{k}} \hat{\gamma}_{\mathbf{k}}^c - v_{\mathbf{k}} \hat{\gamma}_{-\mathbf{k}}^{\dagger c} \right), \quad \hat{a}_{\mathbf{k},\downarrow} = \frac{1}{\sqrt{2}} \left(-\hat{\gamma}_{\mathbf{k}}^s + u_{\mathbf{k}} \hat{\gamma}_{\mathbf{k}}^c - v_{\mathbf{k}} \hat{\gamma}_{-\mathbf{k}}^{\dagger c} \right). \quad (\text{S1})$$

Here we introduce the coefficients $u_{\mathbf{k}} = \sqrt{(\epsilon_{\mathbf{k}} + g_{\text{BB}} n_B)/(2\epsilon_{\mathbf{k}}^c) + 1/2}$ and $v_{\mathbf{k}} = \sqrt{(\epsilon_{\mathbf{k}} + g_{\text{BB}} n_B)/(2\epsilon_{\mathbf{k}}^c) - 1/2}$. The resulting expression for the total Hamiltonian \hat{H} of the system is

$$\begin{aligned} \hat{H} = & g_{\text{IB}}^+ n_B + \frac{\hat{\mathbf{P}}^2}{2m_I} + \sum_{\mathbf{k}} \left(\epsilon_{\mathbf{k}}^c \hat{\gamma}_{\mathbf{k}}^{\dagger c} \hat{\gamma}_{\mathbf{k}}^c + \epsilon_{\mathbf{k}}^s \hat{\gamma}_{\mathbf{k}}^{\dagger s} \hat{\gamma}_{\mathbf{k}}^s \right) + \sqrt{\frac{n_B}{V}} \sum_{\mathbf{k}} \left[g_{\text{IB}}^+ W_{\mathbf{k}} \left(\hat{\gamma}_{\mathbf{k}}^c + \hat{\gamma}_{-\mathbf{k}}^{\dagger c} \right) + g_{\text{IB}}^- \left(\hat{\gamma}_{\mathbf{k}}^s + \hat{\gamma}_{-\mathbf{k}}^{\dagger s} \right) \right] e^{-i\mathbf{k}\hat{\mathbf{R}}} \\ & + \frac{g_{\text{IB}}^+}{2V} \sum_{\mathbf{k},\mathbf{k}'} \left(V_{\mathbf{k}\mathbf{k}'}^{(1)} \hat{\gamma}_{\mathbf{k}'}^{\dagger c} \hat{\gamma}_{\mathbf{k}'}^c e^{i(\mathbf{k}-\mathbf{k}')\hat{\mathbf{R}}} + \hat{\gamma}_{\mathbf{k}'}^{\dagger s} \hat{\gamma}_{\mathbf{k}'}^s e^{i(\mathbf{k}-\mathbf{k}')\hat{\mathbf{R}}} + V_{\mathbf{k}\mathbf{k}'}^{(2)} \hat{\gamma}_{\mathbf{k}'}^{\dagger c} \hat{\gamma}_{\mathbf{k}'}^c e^{i(\mathbf{k}+\mathbf{k}')\hat{\mathbf{R}}} + \text{H.c.} \right) \\ & + \frac{g_{\text{IB}}^-}{V} \sum_{\mathbf{k},\mathbf{k}'} \left(u_{\mathbf{k}} \hat{\gamma}_{\mathbf{k}'}^{\dagger s} \hat{\gamma}_{\mathbf{k}'}^c e^{i(\mathbf{k}'-\mathbf{k})\hat{\mathbf{R}}} - v_{\mathbf{k}} \hat{\gamma}_{\mathbf{k}'}^{\dagger s} \hat{\gamma}_{\mathbf{k}'}^{\dagger c} e^{i(\mathbf{k}'+\mathbf{k})\hat{\mathbf{R}}} + \text{H.c.} \right). \end{aligned} \quad (\text{S2})$$

To simplify the problem, we transform to the frame comoving with the polaron by using the unitary operator $\hat{U} = e^{i\hat{\mathbf{R}}\hat{\mathbf{P}}_B}$ with $\hat{\mathbf{P}}_B = \sum_{\mathbf{k}} \mathbf{k}(\hat{\gamma}_{\mathbf{k}}^{\dagger c} \hat{\gamma}_{\mathbf{k}}^c + \hat{\gamma}_{\mathbf{k}}^{\dagger s} \hat{\gamma}_{\mathbf{k}}^s)$ (we set $\hbar = 1$). This leads to the effective Hamiltonian $\hat{\mathcal{H}} = \hat{U}^\dagger \hat{H} \hat{U}$ given by Eq. (4) in the main text. We note that, in this frame, $\hat{\mathbf{P}}$ becomes the total momentum of the system and commutes with the effective Hamiltonian $\hat{\mathcal{H}}$ and is thus a conserved quantity. We also note that the vertex functions that couple to the spin sector acquire an additional momentum dependence when the SU(2) symmetry of the bath is broken.

The equations of motion and the stationary solution

In this section we provide the full expressions for the equations of motion for the variational parameters, given by Eq. (7) in the main text, and derive their stationary solution. As outlined in the main text, the evolution equations for the amplitudes $\alpha_{\mathbf{k}}^{c,s}$ are given by the variational condition $\delta[\langle \Psi | i\partial_t - \hat{\mathcal{H}} | \Psi \rangle] = 0$ with respect to the product of coherent states (see Eq. (6) in the main text). The resulting equations are

$$\begin{aligned} i\dot{\alpha}_{\mathbf{k}}^c = & \Omega_{\mathbf{k}}^c \alpha_{\mathbf{k}}^c - \frac{\mathbf{k} \cdot (\mathbf{P} - \mathbf{P}_B[\alpha_{\mathbf{k}}^{c,s}])}{m_I} \alpha_{\mathbf{k}}^c + g_{\text{IB}}^+ \left(\sum_{\mathbf{k}'} V_{\mathbf{k}\mathbf{k}'}^{(1)} \alpha_{\mathbf{k}'}^c + \sum_{\mathbf{k}'} V_{\mathbf{k}\mathbf{k}'}^{(2)} \alpha_{\mathbf{k}'}^{*c} \right) \\ & + g_{\text{IB}}^- \left(u_{\mathbf{k}} \sum_{\mathbf{k}'} \alpha_{\mathbf{k}'}^s - v_{\mathbf{k}} \sum_{\mathbf{k}'} \alpha_{\mathbf{k}'}^{*s} \right) + g_{\text{IB}}^+ \sqrt{n_B} W_{\mathbf{k}}, \end{aligned} \quad (\text{S3})$$

$$i\dot{\alpha}_{\mathbf{k}}^s = \Omega_{\mathbf{k}}^s \alpha_{\mathbf{k}}^s - \frac{\mathbf{k} \cdot (\mathbf{P} - \mathbf{P}_B[\alpha_{\mathbf{k}}^{c,s}])}{m_I} \alpha_{\mathbf{k}}^s + g_{\text{IB}}^+ \sum_{\mathbf{k}'} \alpha_{\mathbf{k}'}^s + g_{\text{IB}}^- \left[\sum_{\mathbf{k}'} (u_{\mathbf{k}'} \alpha_{\mathbf{k}'}^c - v_{\mathbf{k}'} \alpha_{\mathbf{k}'}^{*c}) \right] + g_{\text{IB}}^- \sqrt{n_B}, \quad (\text{S4})$$

where \mathbf{P} is the total momentum of the system and $\mathbf{P}_B = \sum_{\mathbf{k}} \mathbf{k}(|\alpha_{\mathbf{k}}^c|^2 + |\alpha_{\mathbf{k}}^s|^2)$. From the rotational symmetry of the system (for the considered case of a polaron at zero momentum, $\mathbf{P} = 0$), the form of our variational wave function, and its initial condition, it follows that we can set $\mathbf{P}_B = 0$ in the course of the time evolution. Thus, as expressed in Eq. (7) in the main text, the above equations reduce to linear inhomogeneous equations for $\alpha_{\mathbf{k}}^{c,s}$, where the last terms on the right-hand-side of Eqs. (S3) and (S4) describe driving forces.

Next, the stationary solution $\bar{\alpha}_{\mathbf{k}}^{c,s}$ is derived by setting the left-hand-sides of Eqs. (S3) and (S4) to zero. From the fact that the real and imaginary parts of the right-hand sides of Eqs. (S3) and (S4) must vanish independently, it follows that the imaginary parts of $\bar{\alpha}_{\mathbf{k}}^{c,s}$ are zero. Then, by solving the coupled integral equations for the remaining real parts of $\bar{\alpha}_{\mathbf{k}}^{c,s}$, we obtain the

stationary solution:

$$\bar{\alpha}_{\mathbf{k}}^c = -\frac{\sqrt{n_B} W_{\mathbf{k}} g_{IB}^+ (1 + g_{IB}^+ B) - (g_{IB}^-)^2 B}{D}, \quad \bar{\alpha}_{\mathbf{k}}^s = -\frac{\sqrt{n_B} g_{IB}^-}{\Omega_{\mathbf{k}}^s D}. \quad (S5)$$

Here we introduce

$$D = (1 + g_{IB}^+ A)(1 + g_{IB}^+ B) - (g_{IB}^-)^2 AB, \quad A = \sum_{\mathbf{k}} \frac{W_{\mathbf{k}}^2}{\Omega_{\mathbf{k}}^c}, \quad B = \sum_{\mathbf{k}} \frac{1}{\Omega_{\mathbf{k}}^s}. \quad (S6)$$

When the interaction between the impurity and the two-component host bosons are not equal, i.e., $g_{IB}^- \neq 0$, the stationary solution $\bar{\alpha}_{\mathbf{k}}^s$ is non-zero and the magnetic polaron is formed.

The energy of the magnetic polaron is given by the expectation value $E_{\text{mpol}} = \langle \Psi_{\text{mpol}} | \hat{\mathcal{H}} | \Psi_{\text{mpol}} \rangle$ with respect to the stationary state $|\Psi_{\text{mpol}}\rangle = \exp [\sum_{\mathbf{k}} (\bar{\alpha}_{\mathbf{k}}^c(t) \hat{\gamma}_{\mathbf{k}}^c + \bar{\alpha}_{\mathbf{k}}^s(t) \hat{\gamma}_{\mathbf{k}}^s - \text{h.c.})] |0\rangle$. Using the solution (S5) and expressing the interaction strengths $g_{IB,\sigma}$ in terms of the scattering lengths $a_{IB,\sigma}$ by the Lippmann-Schwinger equation,

$$\frac{1}{g_{IB,\sigma}} = \frac{m_{\text{red}}}{2\pi a_{IB,\sigma}} - \frac{1}{V} \sum_{\mathbf{k}} \frac{2m_{\text{red}}}{\mathbf{k}^2}, \quad (S7)$$

we obtain

$$E_{\text{mpol}} = \frac{2\pi n_B}{m_{\text{red}} (1/a_{IB}^+ - 1/l_0)}, \quad (S8)$$

where

$$a_{IB}^+ = \frac{a_{IB,\uparrow} + a_{IB,\downarrow}}{2}, \quad l_0 = \left(4\pi \sum_{\mathbf{k}} \frac{1}{\mathbf{k}^2} - \frac{2\pi}{m_{\text{red}}} \sum_{\mathbf{k}} \frac{W_{\mathbf{k}}^2}{\Omega_{\mathbf{k}}^c} \right)^{-1}. \quad (S9)$$

These expressions are fully regularized and the momentum cutoff Λ , introduced in Eq. (S7), can be taken to infinity.

Derivation of the eigenvalue equation

The energy of the magnetic-dressed bound state is given by the eigenvalue equation (9) of the main text. To derive this equation we consider the ansatz

$$|\Psi_b(t)\rangle = \sum_{\mathbf{k}} \left(\psi_{\mathbf{k}}^c(t) \hat{\gamma}_{\mathbf{k}}^{\dagger c} + \psi_{\mathbf{k}}^s(t) \hat{\gamma}_{\mathbf{k}}^{\dagger s} \right) |\Psi_{\text{mpol}}\rangle. \quad (S10)$$

In this state a single phonon and magnon excitation is added to the magnetic polaron $|\Psi_{\text{mpol}}\rangle$ which allows to fully account for the underlying two-body bound states. The equations of motion for $\psi_{\mathbf{k}}^{c,s}$ are derived from the variational condition $\delta[\langle \Psi_b | i\partial_t - \hat{\mathcal{H}} | \Psi_b \rangle] = 0$. They are given by

$$i\dot{\psi}_{\mathbf{k}}^c = (E_{\text{pol}} + \Omega_{\mathbf{k}}^c) \psi_{\mathbf{k}}^c + g_{IB}^+ \sum_{\mathbf{k}'} V_{\mathbf{k}\mathbf{k}'}^{(1)} \psi_{\mathbf{k}'}^c + g_{IB}^- u_{\mathbf{k}} \sum_{\mathbf{k}'} \psi_{\mathbf{k}'}^s, \quad (S11)$$

$$i\dot{\psi}_{\mathbf{k}}^s = (E_{\text{pol}} + \Omega_{\mathbf{k}}^s) \psi_{\mathbf{k}}^s + g_{IB}^+ \sum_{\mathbf{k}'} \psi_{\mathbf{k}'}^s + g_{IB}^- \sum_{\mathbf{k}'} u_{\mathbf{k}'} \psi_{\mathbf{k}'}^c. \quad (S12)$$

In order to find the eigenmodes of these equations, we assume the solutions of the form $\psi_{\mathbf{k}}^{c,s} \propto e^{-i\omega t}$ which oscillate in time with frequency ω . Substituting this ansatz into Eqs. (S11) and (S12), we obtain the equation

$$\begin{pmatrix} 1 - \frac{g_{IB}^+}{2} \Pi_{w^2} & -\frac{g_{IB}^+}{2} \Pi & 0 & -g_{IB}^- \Pi_{uw} \\ -\frac{g_{IB}^+}{2} \Pi & 1 - \frac{g_{IB}^+}{2} \Pi_{w^{-2}} & 0 & -g_{IB}^- \Pi_{uw^{-1}} \\ -\frac{g_{IB}^+}{2} \Pi_{uw} & -\frac{g_{IB}^+}{2} \Pi_{uw^{-1}} & 1 & -g_{IB}^- \Pi_{u^2} \\ 0 & 0 & -g_{IB}^- \Pi_s & 1 - g_{IB}^+ \Pi_s \end{pmatrix} \begin{pmatrix} \sum_{\mathbf{k}} W_{\mathbf{k}} \psi_{\mathbf{k}}^c \\ \sum_{\mathbf{k}} W_{\mathbf{k}}^{-1} \psi_{\mathbf{k}}^c \\ \sum_{\mathbf{k}} u_{\mathbf{k}} \psi_{\mathbf{k}}^c \\ \sum_{\mathbf{k}} \psi_{\mathbf{k}}^s \end{pmatrix} = \begin{pmatrix} 0 \\ 0 \\ 0 \\ 0 \end{pmatrix}, \quad (S13)$$

where we define

$$\begin{aligned}\Pi_{w^{\pm 2}} &= \sum_{\mathbf{k}} \frac{W_{\mathbf{k}}^{\pm 2}}{\omega - E_{\text{mpol}} - \Omega_{\mathbf{k}}^c}, \quad \Pi = \sum_{\mathbf{k}} \frac{1}{\omega - E_{\text{mpol}} - \Omega_{\mathbf{k}}^c}, \quad \Pi_{uw^{\pm 1}} = \sum_{\mathbf{k}} \frac{u_{\mathbf{k}} W_{\mathbf{k}}^{\pm 1}}{\omega - E_{\text{mpol}} - \Omega_{\mathbf{k}}^c}, \\ \Pi_{u^2} &= \sum_{\mathbf{k}} \frac{u_{\mathbf{k}}^2}{\omega - E_{\text{mpol}} - \Omega_{\mathbf{k}}^c}, \quad \Pi_s = \sum_{\mathbf{k}} \frac{1}{\omega - E_{\text{mpol}} - \Omega_{\mathbf{k}}^s}.\end{aligned}\quad (\text{S14})$$

Equation (S13) has nontrivial solutions only if the determinant of the matrix on the left-hand-side vanishes. Expressing the interaction strengths $g_{\text{IB},\sigma}$ in terms of the scattering lengths $a_{\text{IB},\sigma}$ via Eq. (S7) and collecting the leading terms in the limit of $\Lambda \rightarrow \infty$, we obtain the equation (see Eq. (9) in the main text)

$$\left[a_{\text{IB}}^+ - \left(4\pi \sum_{\mathbf{k}} \frac{1}{\mathbf{k}^2} + \frac{2\pi}{m_{\text{red}}} \Pi_s \right)^{-1} \right] \left[a_{\text{IB}}^+ - \left(4\pi \sum_{\mathbf{k}} \frac{1}{\mathbf{k}^2} + \frac{2\pi}{m_{\text{red}}} \frac{\Pi_{w^2} + \Pi_{w^{-2}}}{2} \right)^{-1} \right] = (a_{\text{IB}}^-)^2. \quad (\text{S15})$$

Solving this equation for ω gives the bound state energy ω_{bound} .

Asymptotic scaling of a generation of spin excitations

As shown in the panel II in Fig. 2 in the main text, the number of spin-waves generated obeys an asymptotic \sqrt{t} behavior at long times. This behavior can be understood from a simple scaling argument. For the sake of simplicity, let us neglect interactions between different momentum modes and consider the simplified Hamiltonian where different sectors of momentum \mathbf{k} are decoupled: $\hat{H}_{\mathbf{k}} = \omega_{\mathbf{k}} \hat{\gamma}_{\mathbf{k}}^\dagger \hat{\gamma}_{\mathbf{k}} + V_{\mathbf{k}} (\hat{\gamma}_{\mathbf{k}} + \hat{\gamma}_{\mathbf{k}}^\dagger)$. Here $\hat{\gamma}_{\mathbf{k}}$ denotes a spin or charge annihilation operator at momentum \mathbf{k} and we assume $V_{-\mathbf{k}} = V_{\mathbf{k}}$. In the non-equilibrium problem such as the one studied in this work, the number of excitations $n_{\mathbf{k}}$ in the mode \mathbf{k} will in general oscillate. However, for times larger than $t > 1/\omega_{\mathbf{k}}$, one can give a simple scaling argument for the behavior of $n_{\mathbf{k}}$. At such times, the occupation of excitations have a scaling $\langle \hat{\gamma}_{\mathbf{k}} \rangle \propto V_{\mathbf{k}}/\omega_{\mathbf{k}}$ and thus $n_{\mathbf{k}} \propto (V_{\mathbf{k}}/\omega_{\mathbf{k}})^2$ as can be seen from an inspection of the equation of motion.

Let us then consider the total number of excitations at time t . We identify all modes \mathbf{k} satisfying $\omega_{\mathbf{k}} t > 1$, i.e., the modes $|\mathbf{k}| > k^*$ where k^* is determined by $\omega_{k^*} t = 1$, as contributions to the excitations. Using the estimate $n_{\mathbf{k}} \propto (V_{\mathbf{k}}/\omega_{\mathbf{k}})^2$, we then integrate over these modes to find for the spin excitations

$$N^s(t) = \int d^3 \mathbf{k} n_{\mathbf{k}}^s \propto \int_{k^*}^{\infty} k^2 dk \frac{1}{k^4} \propto \sqrt{t}. \quad (\text{S16})$$

Here we use the fact that for the spin sector $V_{\mathbf{k}} = \text{const.}$, and the magnon dispersion relation scales as $\omega_{\mathbf{k}} \propto k^2$, leading to $k^* \propto 1/\sqrt{t}$. We emphasize that collective excitations satisfying these simple scalings can ubiquitously appear in a variety of systems such as multi-component Bose-Einstein condensates [66, 67], fermionic gases [64, 65], and Rydberg or dipolar gases [68–70].

In contrast, for charge excitations, one has $V_{\mathbf{k}} \propto \sqrt{k}$ and the dispersion is linear $\omega_{\mathbf{k}} \propto k$ at small \mathbf{k} , leading to $k^* \propto 1/t$ and $n_{\mathbf{k}} \propto 1/k$. Hence, if integrated from k^* to infinity, the total number of charge excitations diverges in the ultraviolet (UV) limit. This suggests that the main contribution to N^c comes from the UV limit. At such a large momentum, however, we can use the same scaling argument as for the spin excitations. Since this gives a convergent result in the UV limit, we expect that the number of charge excitations should soon reach a constant number and saturate, in agreement with our numerical findings.

We note that the \sqrt{t} behavior remains observable also in the presence of a small imbalance in the boson-boson scattering length (i.e., broken SU(2) symmetry). In this case, the magnon dispersion relation has a linear low-energy contribution and the number of spin excitations will ultimately saturate. However, since the imbalance in scattering length is typically very small, we expect a large time window for which the \sqrt{t} behavior remains valid before saturation. Specifically, let $t = t^*$ be the time scale at which k^* (determined by $\omega_{k^*} t = 1$) reaches a small value such that the magnon dispersion becomes linear for $k < k^*$. Under this condition, the scaling argument given in Eq. (S16) remains valid as long as $t < t^*$. Hence we expect that t^* is long enough to experimentally observe the \sqrt{t} behavior.

Coupled oscillators dynamics in the presence of two bound states

When two bound states are present (defining the regime III shown in Fig. 1(b) of the main text), the spin and charge excitations exhibit multi-frequency oscillations. Remarkably, continuum modes in the bath mediate a coupling between the two bound states.

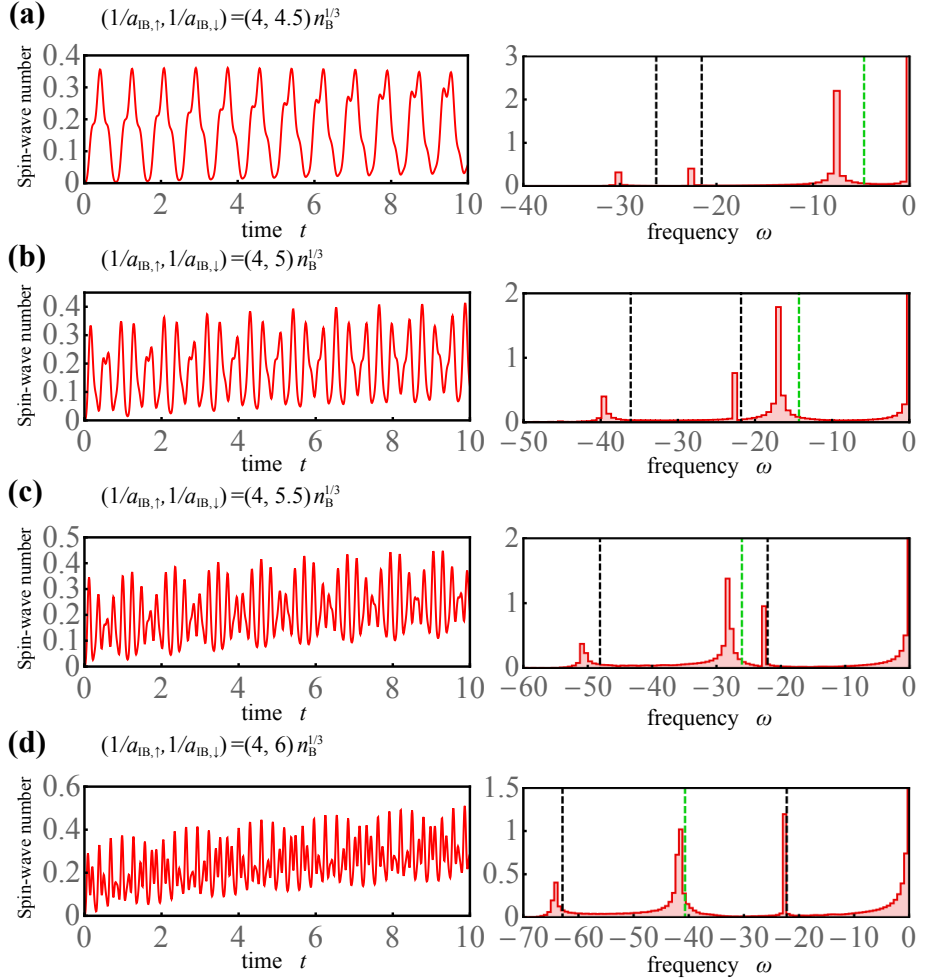


Figure S1. Dynamics of bath spins and their Fourier spectra in the presence of two bound states. One of the scattering lengths is set to $1/(a_{IB,\uparrow} n_B^{1/3}) = 4$ while the other $(1/(a_{IB,\downarrow} n_B^{1/3}))$ is varied in the range from 4.5 to 6 [(a)-(d)]. The black, dashed lines in the Fourier spectra indicate the eigenenergies ω_{bound} of the magnetic bound states calculated from Eq. (9) of the main text, while the green dashed line show the difference of these energies. We use the parameters $a_{BB} n_B^{1/3} = 0.05$ and $m_I/m_B = 0.95$. Time and frequency are shown in units of $m_B/(\hbar n_B^{2/3})$.

As a consequence, the oscillation frequencies found in the spin dynamics are shifted from the “bare” eigenfrequencies that are determined by the magnetic bound state energies given by Eq. (9) in the main text.

To clarify this point further, we show in Fig. S1 the dynamics of bath spins for varying scattering lengths. When both states are weakly bound and close in energy (i.e., both scattering lengths are large and take on similar values), the coupling between the two bound states can be strong enough to induce shifts in the oscillation frequencies as shown in Fig. S1(a). In this regime, a large peak placed at the difference of the two oscillatory modes indicates a strong coupling of the two bound states. As the strength of one of the scattering lengths is decreased, while keeping the other unchanged, the coupling of the two bound states becomes weak and the oscillation frequencies eventually converge to the ‘bare’ bound state energies indicated by the dashed black lines (see Fig. S1(b)-(d)). As the energy gap between both states increases, the gradual decoupling of the two bound states can also be seen as a decrease of the peak height at the difference between the two oscillatory mode energies.

Decoherence induced by a difference in the scattering lengths of host bosons

In the main text, we assumed that the scattering length a_{BB} between host bosons is independent of the spin components $\sigma = \uparrow, \downarrow$. However, in practice, there exists typically a small imbalance in the boson-boson interactions. For example, identifying the hyperfine states $|F = 1, m_F = 1\rangle$ and $|F = 1, m_F = 0\rangle$ as \uparrow -and \downarrow -state, respectively, the imbalance in scattering lengths

is $\sim 0.4\%$ for ^{41}K [75] and $\sim 0.5\%$ for ^{87}Rb atoms [77]. In general, this weak symmetry breaking causes spin decoherence that is additional to the one induced by the impurity. To estimate the size of such a contribution, we consider the Hamiltonian of a two-component gas of host bosons in absence of the impurity

$$\hat{H}_B = \sum_{\mathbf{k}\sigma} \epsilon_{\mathbf{k}} \hat{a}_{\mathbf{k}\sigma}^\dagger \hat{a}_{\mathbf{k}\sigma} + \frac{1}{2V} \sum_{\mathbf{k}, \mathbf{k}', \mathbf{q}} \left(g_{BB\uparrow\uparrow} \hat{a}_{\mathbf{k}+\mathbf{q}, \uparrow}^\dagger \hat{a}_{\mathbf{k}'-\mathbf{q}, \uparrow}^\dagger \hat{a}_{\mathbf{k}, \uparrow} \hat{a}_{\mathbf{k}', \uparrow} + 2g_{BB\uparrow\downarrow} \hat{a}_{\mathbf{k}+\mathbf{q}, \uparrow}^\dagger \hat{a}_{\mathbf{k}'-\mathbf{q}, \downarrow}^\dagger \hat{a}_{\mathbf{k}, \uparrow} \hat{a}_{\mathbf{k}', \downarrow} + g_{BB\downarrow\downarrow} \hat{a}_{\mathbf{k}+\mathbf{q}, \downarrow}^\dagger \hat{a}_{\mathbf{k}'-\mathbf{q}, \downarrow}^\dagger \hat{a}_{\mathbf{k}, \downarrow} \hat{a}_{\mathbf{k}', \downarrow} \right). \quad (\text{S17})$$

Here $g_{BB\sigma\sigma'}$ denotes the interaction strength between host bosons of spin component σ and σ' . Let us introduce imbalance parameters $r_{1,2}$ by

$$g_{BB\uparrow\uparrow} = g_{BB\uparrow\downarrow}(1+r_1), \quad g_{BB\downarrow\downarrow} = g_{BB\uparrow\downarrow}(1+r_2), \quad g_{BB\uparrow\downarrow} \equiv g_{BB}. \quad (\text{S18})$$

Then, by following a similar procedure as outlined in Sec. , we can diagonalize the Hamiltonian to obtain

$$\hat{H}_B = \sum_{\mathbf{k}} \left(\tilde{\epsilon}_{\mathbf{k}}^s \hat{\gamma}_{\mathbf{k}}^{\dagger s} \hat{\gamma}_{\mathbf{k}}^s + \tilde{\epsilon}_{\mathbf{k}}^c \hat{\gamma}_{\mathbf{k}}^{\dagger c} \hat{\gamma}_{\mathbf{k}}^c \right), \quad (\text{S19})$$

where the dispersion relations are given by

$$\tilde{\epsilon}_{\mathbf{k}}^{s,c} = \sqrt{\left(\frac{\mathbf{k}^2}{2m_B} \right)^2 + \frac{gn_B \mathbf{k}^2}{2m_B} \left[\left(1 + \frac{r_1 + r_2}{2} \right) \mp \sqrt{1 + \left(\frac{r_1 - r_2}{2} \right)^2} \right]}. \quad (\text{S20})$$

To ensure that the energies are real, we require that the parameters satisfy the miscible condition:

$$(1+r_1)(1+r_2) > 1 \iff g_{BB\uparrow\uparrow} g_{BB\downarrow\downarrow} > g_{BB\uparrow\downarrow}^2. \quad (\text{S21})$$

The operators $\hat{\gamma}_{\mathbf{k}}^{s,c}$ are related to $\hat{a}_{\mathbf{k},\sigma}$ by a Bogoliubov transformation. As an example, we show the expressions in the case of $r_1 = r_2 = r$:

$$\begin{cases} \hat{a}_{\mathbf{k}\uparrow} = \frac{1}{\sqrt{2}} \left(\tilde{u}_{\mathbf{k}}^s \hat{\gamma}_{\mathbf{k}}^s - \tilde{v}_{-\mathbf{k}}^s \hat{\gamma}_{-\mathbf{k}}^{\dagger s} + \tilde{u}_{\mathbf{k}}^c \hat{\gamma}_{\mathbf{k}}^c - \tilde{v}_{-\mathbf{k}}^c \hat{\gamma}_{-\mathbf{k}}^{\dagger c} \right) \\ \hat{a}_{\mathbf{k}\downarrow} = \frac{1}{\sqrt{2}} \left(-\tilde{u}_{\mathbf{k}}^s \hat{\gamma}_{\mathbf{k}}^s + \tilde{v}_{-\mathbf{k}}^s \hat{\gamma}_{-\mathbf{k}}^{\dagger s} + \tilde{u}_{\mathbf{k}}^c \hat{\gamma}_{\mathbf{k}}^c - \tilde{v}_{-\mathbf{k}}^c \hat{\gamma}_{-\mathbf{k}}^{\dagger c} \right), \end{cases} \quad (\text{S22})$$

where

$$\begin{aligned} \tilde{u}_{\mathbf{k}}^s &= \sqrt{\frac{\mathbf{k}^2}{2m_B} + \frac{gn_B}{2}r} + \frac{1}{2}, \\ \tilde{v}_{\mathbf{k}}^s &= \frac{gn_B r}{2\sqrt{2}} \left[\left(\frac{\mathbf{k}^2}{2m_B} \right)^2 + \frac{gn_B \mathbf{k}^2}{2m_B} r + \left(\frac{\mathbf{k}^2}{2m_B} + \frac{gn_B}{2}r \right) \sqrt{\left(\frac{\mathbf{k}^2}{2m_B} \right)^2 + \frac{gn_B \mathbf{k}^2}{2m_B} r} \right]^{-1/2}. \end{aligned} \quad (\text{S23})$$

For simplicity, we focus on this case in the following. A generalization to the case of $r_1 \neq r_2$ is straightforward and leads to the same qualitative physics.

In order to study how the initially prepared superposition state $|\Psi_{\text{BEC}}\rangle \propto (\hat{a}_{0\uparrow}^\dagger + \hat{a}_{0\downarrow}^\dagger)^{N_B} |0\rangle$ dephases due to the imbalance in the spin-dependent boson-boson scattering lengths, we consider the initial state in terms of the operators $\hat{\gamma}_{\mathbf{k}}^{s,c}$:

$$|\Psi_{\text{BEC}}(0)\rangle \propto \exp \left[\frac{1}{2} \sum_{\mathbf{k} \neq 0} \left(\frac{\tilde{v}_{-\mathbf{k}}^s}{\tilde{u}_{\mathbf{k}}^s} \hat{\gamma}_{\mathbf{k}}^{\dagger s} \hat{\gamma}_{-\mathbf{k}}^s + \frac{\tilde{v}_{-\mathbf{k}}^c}{\tilde{u}_{\mathbf{k}}^c} \hat{\gamma}_{\mathbf{k}}^{\dagger c} \hat{\gamma}_{-\mathbf{k}}^c \right) \right] |0\rangle_{\gamma}, \quad (\text{S24})$$

which satisfies $\hat{a}_{\mathbf{k}\sigma} |\Psi_{\text{BEC}}(0)\rangle = 0$ for $\mathbf{k} \neq 0$, where $|0\rangle_{\gamma}$ denotes the vacuum of the $\hat{\gamma}_{\mathbf{k}}^{s,c}$ operators. From the Hamiltonian (S19), the time evolution of the quantum state follows

$$|\Psi_{\text{BEC}}(t)\rangle \propto \exp \left[\frac{1}{2} \sum_{\mathbf{k} \neq 0} \left(\frac{\tilde{v}_{-\mathbf{k}}^s e^{-2i\tilde{\epsilon}_{\mathbf{k}}^s t}}{\tilde{u}_{\mathbf{k}}^s} \hat{\gamma}_{\mathbf{k}}^{\dagger s} \hat{\gamma}_{-\mathbf{k}}^s + \frac{\tilde{v}_{-\mathbf{k}}^c e^{-2i\tilde{\epsilon}_{\mathbf{k}}^c t}}{\tilde{u}_{\mathbf{k}}^c} \hat{\gamma}_{\mathbf{k}}^{\dagger c} \hat{\gamma}_{-\mathbf{k}}^c \right) \right] |0\rangle_{\gamma}. \quad (\text{S25})$$

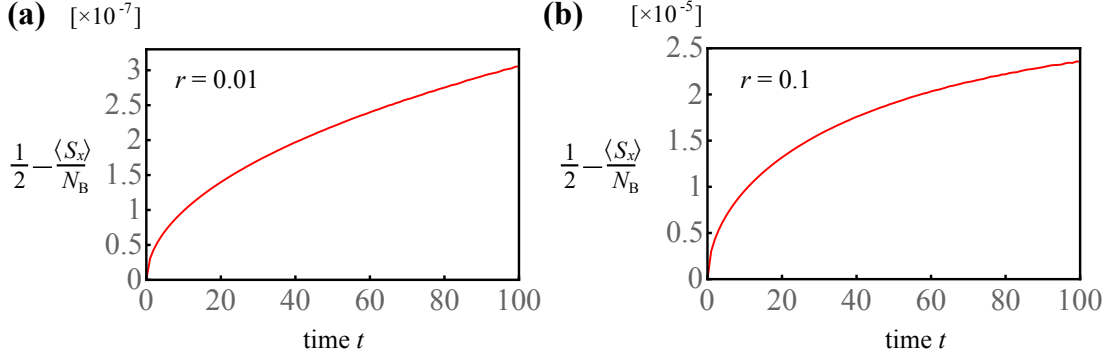


Figure S2. The decoherence induced by an imbalance in the interactions between the different components of the host bosons. The time evolutions are plotted for (a) $r = 0.01$ and (b) $r = 0.1$. The boson-boson interaction is set to $a_{BB}n_B^{1/3} = 0.1$ and we plot time in units of $m_B/(\hbar n_B^{2/3})$.

Then, by denoting $\langle \dots \rangle$ as the expectation value with respect to $|\Psi_{\text{BEC}}(t)\rangle$, the time evolution of the spin operator becomes

$$\frac{\langle \hat{S}_x \rangle}{N_B} = \left\langle \frac{1}{2N_B} \sum_{\mathbf{k}} \left(\hat{a}_{\mathbf{k},\uparrow}^\dagger \hat{a}_{\mathbf{k},\downarrow} + \hat{a}_{\mathbf{k},\downarrow}^\dagger \hat{a}_{\mathbf{k},\uparrow} \right) \right\rangle \quad (\text{S26})$$

$$= \frac{1}{2} - \frac{1}{n_B} \int \frac{d^3 \mathbf{k}}{(2\pi)^3} 2(\tilde{u}_{\mathbf{k}}^s)^2 (\tilde{v}_{\mathbf{k}}^s)^2 (1 - \cos(2\tilde{\epsilon}_{\mathbf{k}}^s t)), \quad (\text{S27})$$

where we used the expressions of the Bogoliubov transformations (S22). The second term in Eq. (S27) represents the decoherence factor induced by the spin-dependent internal interactions between the host bosons. The integral over $(\tilde{u}_{\mathbf{k}}^s)^2$ roughly equals the number of excited particles, which is typically less than 1%, and $\tilde{v}_{\mathbf{k}}^s$ is on the order of r . Thus, the decoherence factor can be estimated by the multiplication of these two factors.

As an example, we assume an imbalance $r = 0.01$. Then the total decoherence factor induced by the internal dynamics (S27) is about $< 10^{-6}$ which is negligible compared to the dephasing induced by the impurity. Figure S2 shows the time evolution of the decoherence given by Eq. (S27) for the imbalance parameters $r = 0.01$, and 0.1. Our numerical finding supports the above estimate of the decoherence factor. In particular, the decoherence is still greatly suppressed even for an imbalance in the boson-boson scattering lengths of about 10%. Thus, our predictions on the magnetic polaron dynamics studied in the main text should be detectable also using a miscible pair of hyperfine states of ^{23}Na by identifying, for instance, $|F = 1, m_F = 1\rangle$ as the \uparrow -state and $|F = 1, m_F = 0\rangle$ as the \downarrow -state, leading to an imbalance $\sim 8\%$ [78]. For this choice, ^{40}K [4] will be the most promising candidate for the impurity atoms.